Supplementary materials

Anchoring and reactivation of single-site Co–porphyrin over TiO_2 for the efficient photocatalytic CO_2 reduction

Chao Zhang,[a] Jiwon Yang,[a] Keisuke Hara,[a] Rento Ishii,[a] Hongwei Zhang,[a] Takaomi Itoi,[b] and Yasuo Izumi[a,*]

[a] *Department of Chemistry, Graduate School of Science, Chiba University, Yayoi 1-33, Inage-ku, Chiba 263-8522, Japan*

[b] *Department of Mechanical Engineering, Graduate School of Engineering, Chiba University, Yayoi 1-33, Inage-ku, Chiba 263-8522, Japan*

1. Experimental

1.1. Photocatalytic CO_2 reduction

The absorbance of Model UV32 (wavelength $\lambda > 320$ nm) [S1], U330 (245 nm $< \lambda <$ 386 nm, and $\lambda > 686$ nm) [S2], and L38 ($\lambda > 380$ nm) filters [S3] are illustrated in each product website.

1.2. Absorption–fluorescence spectra

The absorption–fluorescence spectra were recorded on an FP-8600 spectrofluorometer (JASCO, Tokyo, Japan; Chiba Iodine Resource Innovation Center) equipped with a 150 W Xe arc lamp and a photomultiplier tube in the range of excitation light from 200 to 380 nm and the range of fluorescence light from 200 (or 400) to 800 nm. Before the measurements, the sample powder (2.0 mg) was poured into deionized water (3.0 mL) in a quartz cell and ultrasonicated (430 W, 38 kHz) for 30 min.

1.3. CV measurements

CV measurements were performed to monitor the reduction and oxidation potential of the Co–TCPP complex. A glassy carbon ($\Phi_{\text{polyetheretherketone}}$ 6.0 mm, Φ_{C} 3.0 mm, Model 002012), platinum wire (Model 002222), and Ag/AgCl (Model RE-1B; all three models from BAS Inc., Tokyo, Japan) were used as a working electrode (WE), counter electrode, and reference electrode, respectively. Dimethyl sulfoxide (DMSO) was used as a solvent and the cobalt–tetrakis(4-carboxyphenyl)porphyrin (Co–TCPP) concentration was 1.0 mmol L^{-1}. Tetrabutylammonium perchlorate (0.1 mol L^{-1}) was added as a supporting electrolyte, and 1.0 mmol L^{-1} of ferrocene was added as an internal reference by monitoring the redox of ferrocene/ferrocenium (Fc/Fc^{+}). The WE voltage was swept between –2.5 and 1.0 V versus standard hydrogen electrode (SHE) at a rate of 50 mV s^{-1} using a potentiostat/galvanostat (VersaSTAT 3–100; Princeton Applied Research, Oak Ridge, TN, USA).

1.4. X-ray diffraction (XRD) patterns

XRD patterns were observed using a D8 ADVANCE diffractometer (Bruker, Billerica, MA, USA) at the Center for Analytical Instrumentation at a Bragg angle (θ_B) of $2\theta_B = 5°–80°$ with a scan step of 0.01° and at a rate of 1 s per step. The measurements were performed at 40 kV and 40 mA using Cu Kα emission (wavelength $\lambda = 0.15419$ nm) and a Ni filter.

2. Results and discussion

2.1. Photocatalytic $^{13}CO_2$ reduction and $^{13}CO_2$ exchange

^{13}CO formation rate was 6.3 μmol h^{-1} (Table 2i) using Co–TCPP–TiO_2 (100 mg) under the irradiation of UV–visible light (118 mW cm^{-2}; Model OPM2-502, Ushio, Inc.). We previously

reported the light intensity of the light source, and the light intensity to excite anatase-type TiO_2, i.e. $\lambda < 387$ nm, was 10.4 mW cm^{-2} [S4]. Therefore, the light intensity at the light exit (ϕ = 5.0 cm) was 0.205 J s^{-1}, and if we assume a photon of wavelength of 387 nm, the number was 3.99×10^{17} photons s^{-1}. The obtained rate of 63 μmol h^{-1} g_{cat}^{-1} using 0.100 g of catalyst corresponds to 1.05×10^{15} molecules-CO s^{-1}. We also considered the light absorbed in Co–TCPP–TiO_2 (0.100 g) was one third [S5]. Thus, the quantum yield for the two electron reduction reaction was estimated to $2 \times 1.05 \times 10^{15}$ / ($\frac{1}{3} \times 3.99 \times 10^{17}$ photons s^{-1}) = 1.6%.

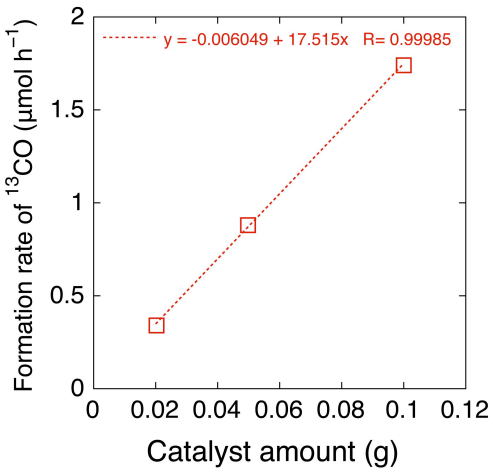

Fig. S1. The dependence of ^{13}CO formation rates (μmol h^{-1}) using $^{13}CO_2$, H_2, Co–TCPP (2.5 wt %)–TiO_2, and UV–visible light on the photocatalyst amount used. The UV–visible light intensity was 118 mW cm^{-2}.

Table S1

Initial CO Formation rates during the first 5 h of reaction using Co–TCPP–TiO_2 (100 mg) under $^{13}CO_2$ (2.7 kPa), H_2 (20.7 kPa), and UV–visible light irradiation. The UV–visible light intensity was 118 mW cm^{-2}.

Entry	Co–TCPP loading (wt %)	Formation rate (μmol h^{-1} g_{cat}^{-1})			^{12}CO ratio (mol%)
		^{13}CO	^{12}CO	Σ CO	
a	1.0	1.9	0.45	2.4	19
b	2.5	17	7.1	25	29
c	5.0	7.0	6.5	14	48
d	7.5	5.7	3.3	9.0	36
e	25	0.27	0.27	0.53	50

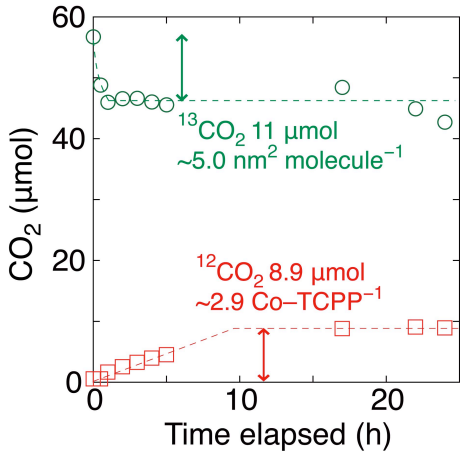

Fig. S2. Time-course uptake of $^{13}CO_2$ (0.67 kPa) and partial decomposition of Co–TCPP irradiated under UV–visible light using Co–TCPP (2.5 wt %)–TiO_2. Photocatalyst used was 0.100 mg and the UV–visible light intensity was 118 mW cm^{-2}.

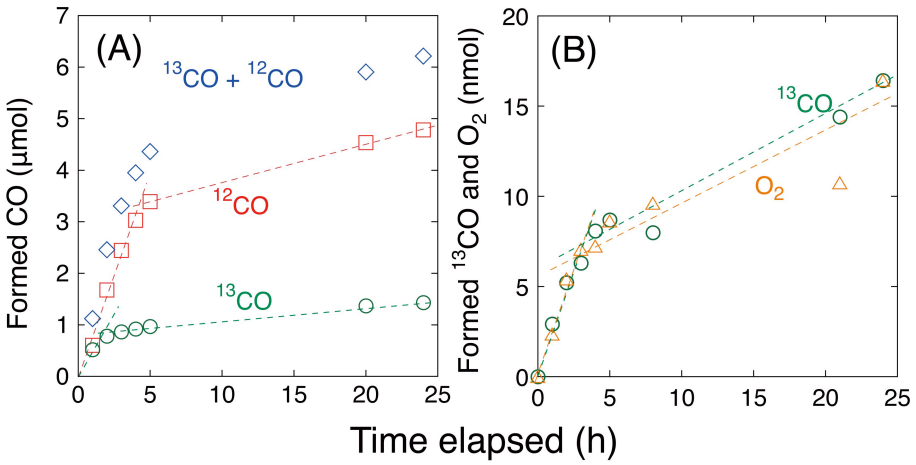

Fig. S3. Time-course formation of photocatalytic ^{13}CO and ^{12}CO during exposure to $^{13}CO_2$ (2.7 kPa) and H_2O (1.7 kPa) using (A) Co–TCPP (2.5 wt %)–TiO_2 (anatase phase, JRC-TIO14) and (B) Co–TCPP (2.5 wt %)–TiO_2 (rutile phase, JRC-TIO6) under UV–visible light irradiation. Photocatalyst amount was 100 mg and the UV–visible light intensity was 118 mW cm^{-2}.

2.2. Absorption–fluorescence spectra

The fluorescence spectra of the Co–TCPP–TiO_2 composite with the excitation at 200 nm are shown in Fig. S2A. The major peak at 376 nm was attributed to the band gap emission (3.2 eV) of anatase-phase TiO_2. As the Co–TCPP content in the sample was increased, the major peak as well as a shoulder peak at 396 nm progressively diminished, demonstrating effective electron transfer from the conduction band of TiO_2 into the HOMO of Co–TCPP. Three weak peaks at 452, 468, and 529 nm for TiO_2 (curve A in Fig. S4) were due to the electron transition from or to the middle-gap trapping states on/in TiO_2, e.g., surface O vacancy [S6]. The intensity of these peaks also decreased with an increase of Co–TCPP content, suggesting electron transfer from or to such trap states to or from Co–TCPP electronic orbital state (Scheme 2A).

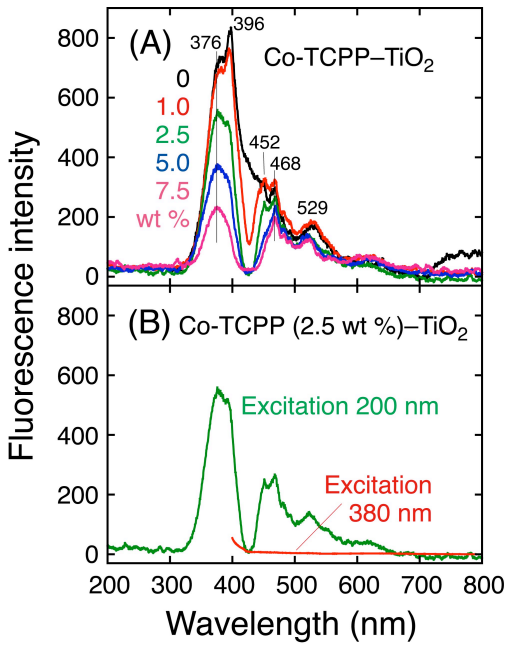

Fig. S4. Fluorescence spectra of (A) Co–TCPP–TiO_2 composite with various amounts of Co–TCPP (0, 1.0, 2.5, 5.0, and 7.5 wt %) with the excitation wavelength at 200 nm and (B) Co–TCPP (2.5 wt %)–TiO_2 composite with the excitation wavelength at 200 and 380 nm.

When the excitation wavelength was changed to 380 nm, the fluorescence intensity became essentially zero in the wavelength range of 400–800 nm (Fig. S2B), indicating that the fluorescence from the composites exclusively originated from the relaxation of excitations in TiO_2 rather than the HOMO–LUMO relaxation of porphyrins.

2.3. CV results

The reduction and oxidation of Co–TCPP were monitored by CV (Fig. S5). In comparison with the Fc/Fc^+ pair at mean 0.52 V (versus SHE) that is close to the value in literature (0.422 V) [S7], the redox pair at mean –0.79 V can be assigned to the redox at LUMO [e_g*(π), Scheme 2], dispersing over the porphyrin ring: on the N atoms of pyridine rings and C atoms of connecting CH part rather than localized at Co^+/Co^{2+} [S8].

The redox pair at mean –1.89 V can be assigned to LUMO + 1 [e_u*(π)], dispersing over the benzene rings of porphyrin (Scheme 2B) rather than localized Co^0/Co^{1+} [S8]. On the basis of the Q band and Soret band peak positions (Fig. 2B), HOMO [a_{2u}(π)] and HOMO – 1 [a_{1u}(π)] levels were determined (Scheme 2A).

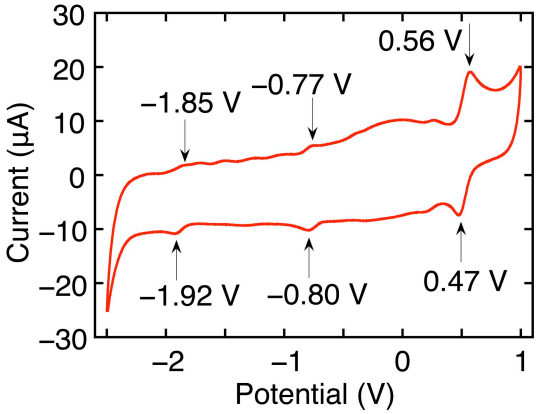

Fig. S5. CV for Co–TCPP dissolved in DMSO.

2.4. XRD patterns

XRD patterns of Co–TCPP (0, 1.0, 2.5, 5.0, and 7.5 wt %)–TiO_2 composites (Fig. S6) were measured. The peaks at 25.2°, 37.6°, 47.7°, 54.5°, 62.4°, 69.1°, and 75.0° can be assigned to the diffraction in the 1 0 1, 0 0 4, 2 0 0, 2 1 1, 2 0 4, 1 1 6, and 2 1 5 planes, respectively, of anatase-type TiO_2 [S9]. No obvious peaks due to Co–TCPP appeared, suggesting that the stacking repetition of J- and/or H-aggregation is limited which could not result in a crystal-like structure on the TiO_2 surface.

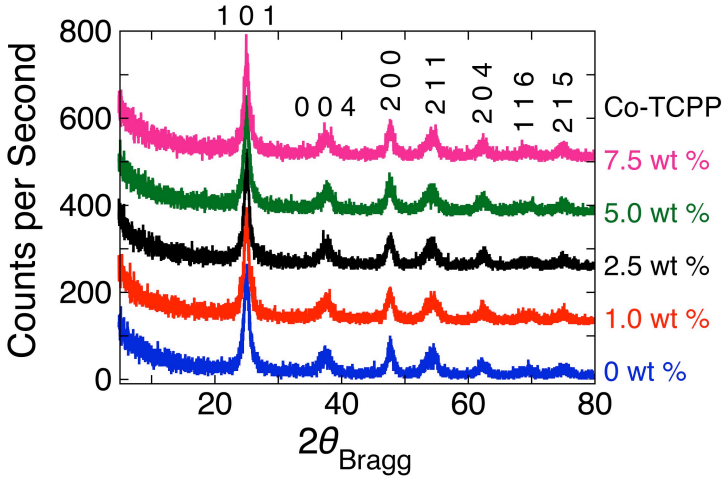

Fig. S6. XRD patterns of the Co–TCPP–TiO_2 composites with various amounts of Co–TCPP (0, 1.0, 2.5, 5.0, and 7.5 wt %).

2.5. HR-TEM

The crystal parameters for anatase-phase TiO_2 were based on ref. S10 for the assignment of lattice fringes in HR-TEM (Fig. 5).

2.6. EXAFS spectra

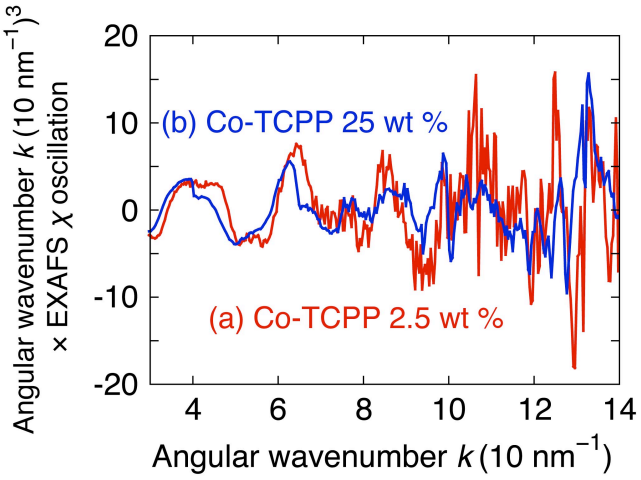

Fig. S7. (a) Comparison of angular wave number k^3-weighted EXAFS χ oscillation between (a) fresh Co–TCPP (2.5 wt %)–TiO_2 measured in fluorescence detection mode and (b) fresh Co–TCPP (25 wt %)–TiO_2 measured in transmission mode both at the Co K-edge.

2.7. Reactivation of Co–TCPP (2.5 wt %)–TiO_2 catalyst

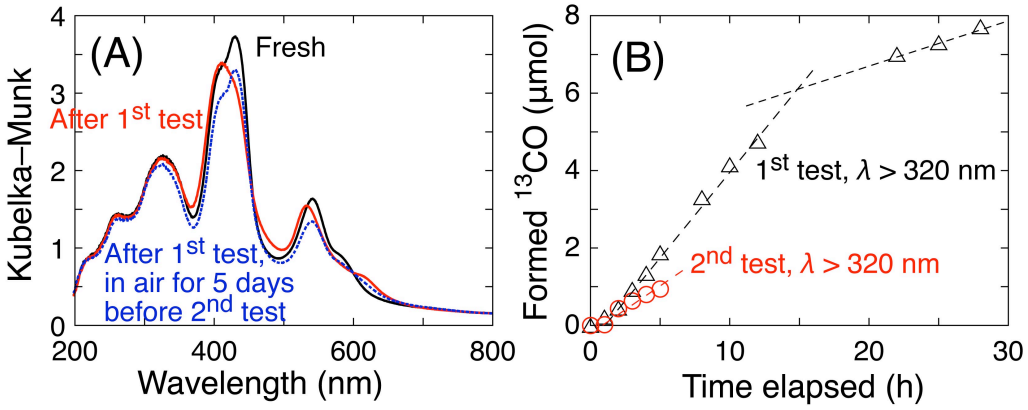

Fig. S8. (A) UV–visible absorption spectra of Co–TCPP (2.5 wt %)–TiO_2 used for reaction under the irradiation of UV–visible light of $\lambda > 320$ nm, before reaction (black), after reaction (red), and set aside for 5 days (blue). (B) Time course of ^{13}CO formation using Co–TCPP (2.5 wt %)–TiO_2 under $\lambda > 320$ nm in the first (black) and second photoreduction tests of $^{13}CO_2$ (red). Photocatalyst amount was 100 mg.

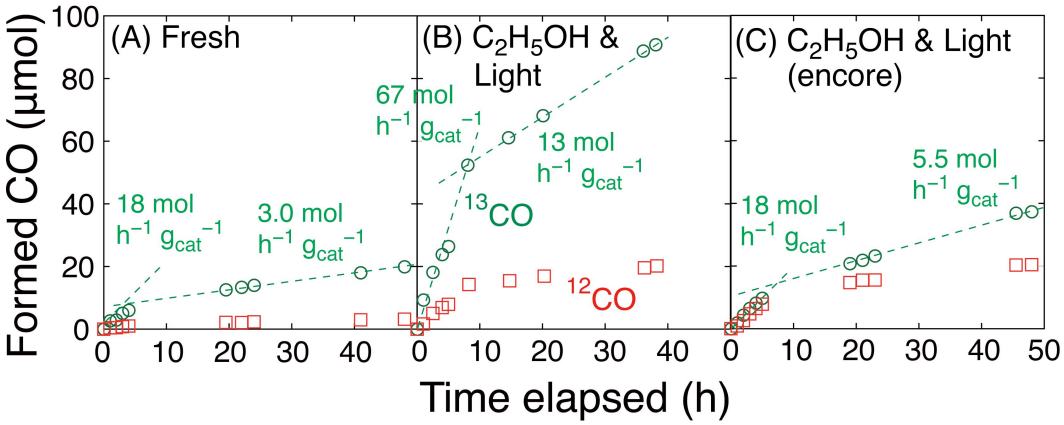

Fig. S9. Time-course formation of photocatalytic ^{13}CO and ^{12}CO during exposure to $^{13}CO_2$ (2.7 kPa) and H_2 (20.7 kPa) using (A) Co–TCPP (2.5 wt %)–TiO_2 under UV–visible light, (B) Co–TCPP (2.5 wt %)–TiO_2 used for the test in panel A was treated with ethanol (2.7 kPa) for 5 min and irradiated under UV–visible light and was reused, and (C) Co–TCPP (2.5 wt %)–TiO_2 used for the test in panel B was treated with ethanol (2.7 kPa) for 5 min and irradiated under UV–visible light and was reused. Photocatalyst amount was 100 mg and the UV–visible light intensity was 118 mW cm^{-2}.

References

[S1] http://www.newportglass.com/hoyuv32.htm (checked on February 27, 2022).

[S2] https://www.hoyacandeo.co.jp/japanese/products/eo/color/10.html (checked on February 27, 2022).

[S3] https://www.hoyacandeo.co.jp/japanese/products/eo/color/01.html (checked on February 27, 2022).

[S4] H. Zhang, S. Kawamura, M. Tamba, T. Kojima, M. Yoshiba, Y. Izumi, Is Water More Reactive Than H_2 in Photocatalytic CO_2 Conversion into Fuels Using Semiconductor Catalysts under High Reaction Pressures? J. Catal. 352 (2017) 452–465.

[S5] Y. Yoshida, Y. Mitani, T. Itoi, Y. Izumi, Preferential Oxidation of Carbon Monoxide in Hydrogen Using Zinc Oxide Photocatalysts Promoted and Tuned by Adsorbed Copper Ions, J. Catal. 287 (2012) 190–202.

[S6] D. Pan, N. Zhao, Q. Wang, S. Jiang, X. Ji, L. An, Facile Synthesis and Characterization of Luminescent TiO_2 Nanocrystals, Adv. Mater. 17 (2005) 1991–1995.

[S7] G. Pu, Z. Yang, Y. Wu, Z. Wang, Y. Deng, Y. J. Gao, Z. Zhang, X. Lu, Investigation into the Oxygen-Involved Electrochemiluminescence of Porpyrins and Its Regulation by Peripheral Substituents/Central Metals, Anal. Chem. 91 (2019) 2319–2328.

[S8] A. N. Marianov, A. S. Kochubei, T. Roman, O. J. Conquest, C. Stampfl, Y. Jiang, Resolving Deactivation Pathways of Co Porphyrin-Based Electrocatalysts for CO_2 Reduction in Aqueous Medium, ACS Catal. 11 (2021) 3715–3729.

[S9] K. Thamaphat, P. Limsuwan, B. Ngotawornchai, Phase Characterization of TiO_2 Powder by XRD and TEM. Kasetsart J. (Nat. Sci.) 42 (2008) 357–361.

[S10] B. G. Hyde, S. Andersson, Inorganic Crystal Structures, John Wiley & Sons, New York, USA, 1989, p 14.